# Structure and Optical Bandgap Relationship of π-Conjugated Systems

**André Leitão Botelho, Yongwoo Shin, Jiakai Liu, Xi Lin***

Department of Mechanical Engineering and Division of Materials Science and Engineering, Boston University, Boston, Massachussetts, United States of America

## Abstract

In bulk heterojunction photovoltaic systems both the open-circuit voltage as well as the short-circuit current, and hence the power conversion efficiency, are dependent on the optical bandgap of the electron-donor material. While first-principles methods are computationally intensive, simpler model Hamiltonian approaches typically suffer from one or more flaws: inability to optimize the geometries for their own input; absence of general, transferable parameters; and poor performance for non-planar systems. We introduce a set of new and revised parameters for the adapted Su-Schrieffer-Heeger (aSSH) Hamiltonian, which is capable of optimizing geometries, along with rules for applying them to any π-conjugated system containing C, N, O, or S, including non-planar systems. The predicted optical bandgaps show excellent agreement to UV-vis spectroscopy data points from literature, with a coefficient of determination $R^2 = 0.95$, a mean error of $-0.05$ eV, and a mean absolute deviation of 0.16 eV. We use the model to gain insights from PEDOT, fused thiophene polymers, poly-isothianaphthene, copolymers, and pentacene as sources of design rules in the search for low bandgap materials. Using the model as an in-silico design tool, a copolymer of benzodithiophenes along with a small-molecule derivative of pentacene are proposed as optimal donor materials for organic photovoltaics.

## Introduction

One principal goal of condensed matter theory is to understand the structure-property relationship of materials systems such that specific materials properties may be achieved via molecular design. The emergence of fascinating applications using π-conjugated polymers in light-emitting devices [1] and photovoltaics [2] requires precise control and flexible tuning of optical bandgaps to effectively cover the visible and other parts of the solar spectrum. In particular for photovoltaics, Scharber et al. [3] has derived an empirical formula for the power conversion efficiency (PCE) as a function of the optical gap and the relative LUMO level of the donor material. Existing π-conjugated systems that have optimal bandgaps are still rare. [4,5].

The optical bandgap of organic molecules can be qualitatively derived from its dependence on the bond length alternation pattern, planarity, aromaticity, and/or electron-withdrawing/releasing substitutions. [4] Although useful in describing certain trends, these properties are ultimately dependent on the electronic structure of the molecule, which must hence be incorporated in any accurate quantitative description. Predicting the optical bandgaps of optoelectroactive materials accurately is challenging because in principle it requires knowledge of the two-particle Green's function propagator. [6] As one of the most successful quantum many-body theories, the first-principles density functional theory (DFT) guarantees only the ground-state properties, [7,8] and due to the convex nature of the energy functionals at fractional charge states [9] DFT fails to predict fundamental electron localizations in a few strongly correlated materials systems. [10] One of these difficult cases concerns the self-localized soliton and polaron states in conjugated polymers, [11] for which even the time-dependent DFT [12] under the adiabatic local density approximation is known to fail in the extended polymer limit. [13].

Simpler quantum mechanical approaches that are computationally less expensive and can give good bandgap values for specific systems can be divided into two groups. The first group, including for example the Hückel, [14] extended-Hückel, [15] and Valence Effective Hamiltonian, [16,17] do not properly model the electron-phonon coupling that gives rise to the fundamental excitations (solitons, polarons, and bipolarons) of conducting polymers. Furthermore, these models typically rely on external input from semi-empirical or *ab-initio* calculations for the molecular geometries, [18] defeating the computational cost benefit of using a simpler model.

The second group of models includes electron-phonon interactions and can predict the fundamental excitations of conjugated systems, while simultaneously optimizing the molecular geometries. This group includes the Su-Schrieffer-Heeger model [19] and the related Longuet-Higgins Salem (LHS) model. [20] Although there has been some effort in parameterizing the LHS model for heteroatoms, [21,22] we are not aware of any study that has validated the transferability of the parameters across more than a few closely related systems.

In our previous works [23,24], we developed the adapted Su-Schrieffer-Heeger (aSSH) Hamiltonian and demonstrated its accuracy to be better than that of TDDFT, while still correctly describing polarons and their effects, as well as photoinduced charge transfer when π-π stacking inter-chain terms are added. [25] We have chosen to neglect explicit correlations, which may be needed to describe a few phenomena such as negative spin-density waves [26], multiple gap states [27], and 3D conformation couplings [28], in favor of a simpler model that can be solved quickly through a single diagonalization of the Hamiltonian. The underlying physics is to universally re-normalize the strong electron correlations into the effective electron-phonon couplings so that the phonon-dressed quasi-particles can be created across all these different types of π-conjugated systems under the Fermi liquid theory. [11,19].

Nevertheless, until now we had only demonstrated the transferability of the aSSH model for different chain lengths of the very polymers used to determine the parameters. For example, the parameters for sulfur were fit using the optical gap from α-sexithiophene and high level electronic structure calculations for the geometry of the thiophene monomer, but transferability was only shown for the series of oligothiophenes of differing chain lengths. In this work, we not only determine new sets of parameters to extend the scope of the model, but we also demonstrate their transferability by predicting the optical bandgaps for 198 π-conjugated systems representing a wide range of π-conjugated structures.

To exemplify our intended utility of the model as an in-silico design tool, we focus on the problem of finding an appropriate donor material for bulk heterojunction (BHJ) photovoltaic devices. In these BHJ devices, the electron donor absorbs photons to create electron-hole pairs while the acceptor material draws the electrons but not the holes from the donor. The number of photons absorbed that generate charge carriers directly contributes to the short circuit current ($I_{sc}$) of the device. Since only photons with energy higher than the optical gap can be absorbed, a smaller gap leads to a higher current. However, higher energy excitations eventually relax down to the LUMO of the acceptor, so the open circuit voltage ($V_{oc}$) can never be larger than the difference between the LUMO of the acceptor HOMO of the donor. Since the power output, and hence the PCE, is explicitly dependent on $I_{sc} * V_{oc}$, and reducing the optical gap increases $I_{sc}$ but reduces $V_{oc}$, there is an optimal gap for any device that maximizes the PCE. Scharber et al. [3] has derived an empirical formula for the PCE as a function of the donor's optical gap and the relative LUMO levels of the donor and acceptor materials. Assuming a suitably matched acceptor material, the most important intrinsic property to improve PCE becomes the optical gap. From Scharber's analysis, an optimal range for the optical gap lies between 1.2 and 1.5 eV, close to the Shockley-Queisser model result of 1.1 eV for inorganic p-n single junction solar cells. [29] Analyzing the aSSH model predictions to understand which structure modifications lead to lower optical gaps, we propose two new π-conjugated structures with a potential for the optimal 1.2 eV optical bandgap for single junction devices [3,29]: one suitable for polymer solar cells [30,31] and the other for small-molecule crystalline solar cells. [32].

## Computational Methods

The aSSH Hamiltonian [23] used in this work can be written as

$$H = -\sum_{ij} \left[ \gamma t_0 - \sqrt{\gamma}\alpha(b_{ij} - b_{ij}^0) \right](C_i^+ C_j + C_j^+ C_i)$$
$$-\varepsilon \sum_i C_i^+ C_i + \sum_{ij} \frac{K}{2}\left[ b_{ij} - b_{ij}^0 - \frac{4\sqrt{\gamma}\alpha}{\pi K} \right]^2,$$

where $b_{ij} = |\mathbf{r}_i - \mathbf{r}_j|$ is the bond length between the $i^{th}$ and $j^{th}$ atomic sites located at $\mathbf{r}_i$ and $\mathbf{r}_j$ respectively, with the corresponding dummy reference $b_{ij}^0$. [23] The original SSH constants include the σ-bond spring constant $K = 21$ eV/Å$^2$, the reference hopping integral $t_0 = 2.5$ eV, and the linear electron-phonon coupling constant $\alpha = 4.1$ eV/Å. [19] $C_i^+$ and $C_i$ are the creation and annihilation operators for the π-electron at site $i$, respectively. The dimensionless $\gamma$ scales the hopping integral parameters as $\gamma t_0$ and $\sqrt{\gamma}\alpha$ so that $\gamma \neq 1$ for all bonded pairs that include heteroatoms or are part of six-membered aromatic rings. Such a choice of electron-phonon scaling ensures that the universal electron-phonon coupling constant [11] $\lambda = 2\alpha^2/\pi K t_0$ and the σ-bond spring constant $K$ are unaltered for all conjugated bonds, which means all of the π-electrons are treated on an equal footing. ε denotes the density operator $C_i^+ C_i$ strength so that $\varepsilon > 0$ attracts more electrons onto the heteroatomic sites as compared to the carbon reference where $\varepsilon = 0$.

The fully transferable $\gamma$ and $\varepsilon$ values summarized in Table 1 are used for all the π-conjugated systems discussed in this work. Except for the polymer-fullerene heterojunctions, our calculations are performed on finite-sized, isolated molecules and compared with the optical bandgaps from oligomers and polymers in dilute solutions (with only PBDTDTBT [33,34] and PFDTTPDB [35] from thin film), for which the inter-chain steric effects are minimized. The heterojunctions require additional π-π stacking Hamiltonians as discussed separately by Shin and Lin. [25] The determination of the parameters for N̈, S̈, and benzene bonds is discussed in our previous works [23,24], while the values for Ö we now re-determine using the widely overlooked lowest energy UV-vis absorption peak from polyfuran (PFu). [36] Newly determined for this work are the parameters for Ṅ using pyridine, [37] Ȯ using thieno[3,4-c]pyrrole-4,6-dione polymer, [38] and the bridge $\gamma$ for perpendicular fused rings using poly-isothianaphthene. [39,40] The new parameters for heteroatoms are unambiguously determined using the same methodology as our previous work, namely using a single optical gap point from a well characterized oligomer and the bond dimerization magnitude from a monomer calculated with either the quadratic configuration interaction with single and double substitutions (QCISD). [41] The new parameter for bridge bonds, which are dependent on the structure of the connected monomers, is discussed under the perpendicular fused rings section of the results and discussion. We also change the parameters for poly-(p-phenylene vinylene) (PPV), [42] poly-(p-phenylene) (PPP), [43] and polyacenes[44–50] to $\gamma = 1.16$ and $\varepsilon = 0$ from benzene in order to simply the rules for applying the model, where these parameters are now applied to any 6-membered aromatic carbon ring, regardless of whether it is benzene, a phenyl group, or it is fused with other rings. In the case where a bond is part of two fused rings, if one of the rings is a six-membered carbon ring the parameters from benzene are still applied. The $\gamma$ parameter for any bond between two heteroatoms is taken as the $\gamma$ from the heteroatom with the heavier mass.

**Table 1.** aSSH parameters.

|  | $\gamma$ | $\varepsilon$ (eV) |
|---|---|---|
| $\ddot{N}$ | 1.47[a] | 4.36[a] |
| $\dot{N}$ | 1.05 | 0.59 |
| $\ddot{O}$ | 1.44 | 5.46 |
| $\dot{O}$ | 1.07 | 0.34 |
| $\ddot{S}$ | 1.15[a] | 2.85[a] |
| Benzene | 1.16[a] | 0[a] |
| Bridge between for perpendicular 2-rings | 0.75 | – |
| Bridge between perpendicular 3-rings | 0.20 | – |
| All other $\dot{C}$ | 1[b] | 0[b] |

Dots over elements specify the number of $\pi$-electrons contributed to the conjugated system. C-C bonds in six-membered aromatic rings and the bridge bonds between perpendicular fused rings require $\gamma \neq 1$.
[a]Reference: [24].
[b]Original parameters from [19].

## Results and Discussion

Since all of the experimental data are taken from UV-vis absorption spectra reported in literatures, we will focus solely on the optical bandgaps as opposed to either the electronic or transport bandgaps. Fig. 1 shows the agreement between the optical bandgaps predicted by the aSSH model and those measured by UV-vis experiment, where perfect agreement lying on the central dashed line and $\pm 10\%$ within the solid lines. The predicted bandgaps have an overall coefficient of determination of $R^2 = 0.96$, a mean error $ME = -0.05$ eV with a mean absolute deviation of $MAD = 0.16$ eV. Numerical tables of all the calculated versus experimental optical gaps along with references and chemical structures can be found in the Supporting Information, Tables S1–6 and Figures S1–6. The $\pi$-conjugated systems summarized in Fig. 1 are grouped into six categories according to their constituent monomer units, each shown individually in subplots in Fig. 2: a) simple aromatic rings (gray squares) such as polythiophene (PTh), polypyrrole (PPy), PFu, PPP, PPV, and *etc*.; b) fused aromatic rings parallel to the conjugated path direction (red circles); c) fused aromatic rings perpendicular to the conjugated path direction (blue diamonds); d) copolymers from polymerization of any of the previous groups (yellow triangles pointing downwards); e) polycyclic aromatic hydrocarbons (PAHs) including polyacenes where the conjugated paths are greater than one dimension (violet triangles pointing upwards); and f) systems with explicit interchain $\pi$-$\pi$ interactions with fullerene and PPV bulk structures (gray crosses). Guided by insights from each category, we make recommendations for both small molecule and polymer optoelectro-devices operating at the 1.20 eV bandgap target, [3,29] as well as $\pi$-conjugated materials with bandgaps as low as 0.8 eV for long wavelength absorbing materials used in tandem cells.

### Simple Aromatic Rings

The agreement between the calculated and experimental gaps are shown in Fig. 2a and has the best fit of any of the groups here, with $R^2 = 0.97$, $ME = -0.09$ eV, and $MAD = 0.14$ eV. Out of the 67 included here, one point for each of PTh, PFu, PPy, and pyridine were used as targets for fitting $\ddot{S}, \ddot{O}, \ddot{N}$, and $\dot{N}$, respectively, and hence have zero error. Removing these points from the data set increases the $MAD$ by 0.01 eV but has no
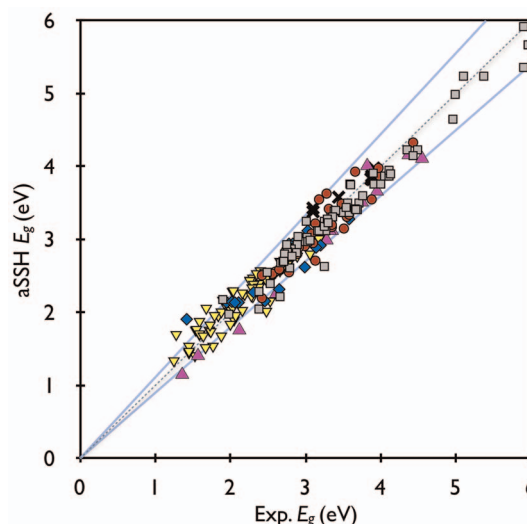


**Figure 1. Predicted aSSH optical bandgaps are compared with experimental ones for 198 independent $\pi$-conjugated systems.** Subgroups include simple rings (Gray squares), parallel fused rings (red circles), perpendicular fused rings (blue diamonds), copolymers (yellow down-triangles), PAHs (violet up-triangles), and $\pi$-$\pi$ stacking systems (gray crosses). Dashed and solid lines are $\pm 0\%$ and $\pm 10\%$ deviations from experimental values, respectively. The coefficient of determination of $R^2 = 0.96$, mean error $-0.05$ eV, and mean absolute deviation 0.16 eV.
doi:10.1371/journal.pone.0086370.g001

significant effect on $ME$ or $R^2$. Considering the extended polymer limit, for which the $\pi$-conjugation length $N \to \infty$, the optical bandgaps decrease from 3.64 eV for PPP, 3.05 eV for PPy, 2.83 eV for PFu, 2.63 eV for PTh, to 2.54 eV for PPV. [24] Further decreases in the bandgaps have been pursued through structural modifications, [4] typically starting from PTh and PPV as they have the lowest bandgaps of the group, in an effort to achieve the optimal gap of 1.20 eV. [51].

One straightforward way to modify the bandgap of PTh is to replace the $\beta-$hydrogens with side-groups that will affect the $\pi$-conjugation. Such is the case of the widely used poly-3,4-ethylenedioxythiophene (PEDOT), in which two oxygens are conjugated to the two $\beta$-C sites of PTh. Note that PEDOT is different from the perpendicular fused aromatic rings (to be discussed below) in that these oxygens are not part of an aromatic ring. As shown in Fig. 3, the lower optical bandgap of PEDOT, $E_g(N = 80) = 2.18$ eV as compared to 2.66 eV for PTh, is caused by the two new oxygen (O) bands lying below the ring (R) band [23]. These two O bands consist of all the $\pi$-binding states between the O and $\beta$-C sites, which push the remaining anti-bonding states, i.e. O and $\beta$-C having opposite phases, upwards in energy. Because the valence (V) band has larger wavefunction components on the $\beta$-C sites than the conduction (C) band, the corresponding highest occupied molecular orbital (HOMO) of PEDOT moves upwards in energy more than the lowest unoccupied molecular orbital (LUMO). Therefore, the bandgap of PEDOT decreases.

### Parallel Fused Rings

Starting from PTh, one popular way in which researchers have been attempting to lower the bandgaps is to fuse adjacent rings by adding extra conjugated sulfur bridges. [4] The argument commonly used to justify this idea is planarization of the $\pi$-conjugated path, which may be misleading because a system with
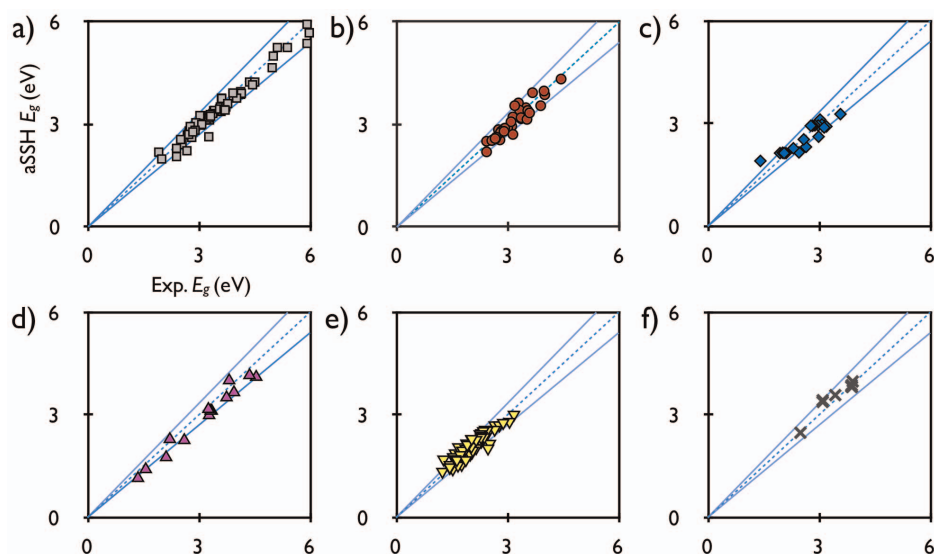
**Figure 2. Subgroups of calculated bandgaps compared to experimental: a) simple rings, b) parallel fused rings, c) perpendicular fused rings, d) copolymers, e) PAHs, and f) $\pi$-$\pi$ stacking systems.** Dashed and solid lines are $\pm 0\%$ and $\pm 10\%$ deviations from experimental values, respectively.
doi:10.1371/journal.pone.0086370.g002

a non-planar configuration is indicative of weak electron hopping across long bridge bonds [52] and does not necessarily imply a large bandgap.

For a given $\pi$-conjugation length, say $N = 120$ as depicted in Fig. 4a, one may vary the number and positioning of sulfur groups to construct a series of polymers with different numbers of fused thiophene rings $N_{FR}$ in monomers. For example, PTh of $N_{FR} = 1$ (Fig. 4b) can be seen as poly-thienoacene (PTA) of $N_{FR} = \infty$ (Fig. 4d) after removal of every other sulfur atom; removing every third sulfur atom in PTA gives poly-thieno[3,2-b]-thiophene



**Figure 3. Density of states (DOS) and wavefunctions of all the $\pi$-bands of PTh and PEDOT, both containing 20 monomer units.** In addition to the ring (R), localized (L), valence (V), conduction (C), and other bands of higher energies (wavefunctions not shown) of PTh, the two low-lying oxygen (O) bands that are formed in PEDOT push the remaining bands, which have nodes between the O and $\beta$-C sites, upwards in energy. The HOMO level (top of the V band) increases in energy more than the LUMO level (bottom of the C band) because the former has larger wavefunction components on the $\beta$-C sites. This effectively lowers the optical bandgap of PEDOT, as compared to PTh.
doi:10.1371/journal.pone.0086370.g003

(PT32bT) of $N_{FR} = 2$ (Fig. 4c); etc. Experimental data from polymers including one, two and three thiophene rings in a single monomer, as well as short PTA's, are compared with aSSH calculations in Fig. 2b and have $R^2 = 0.87$, $ME = -0.07$ eV, and $MAD = 0.14$ eV.

It is clear from Fig. 4e that the bandgap variation for conjugated polymers consisting of parallel fused thiophene rings does not follow the planarization argument. Instead, we find that PT32bT has the lowest bandgap and PTA has the highest while PTh is essentially in the middle. At this point, one may be tempted to put planarization aside and recall that the bandgap of *trans*-poly-acetylene (tPA), the prototypical conducting polymer, is proportional to its bond-length dimerization amplitude. [11] This simple rule, however, does not hold for conjugated polymers containing aromatic rings or even more complicated conjugated structures. [23] The bond-length dimerization amplitude does not follow the same trend and thus cannot satisfactorily describe it. Such non-monotonic variation in $E_g$ is caused by the wavefunction symmetries and energy band crossovers of the LUMO and HOMO levels as follows.

Since PTh has a LUMO orbital (Fig. 3, C band) with large wavefunction components on the sulfur, which is anti-bonding to the two neighboring $\alpha$-C sites, $E_{LUMO}$ is sensitive to the total amount of such unfavorable electron hopping. As shown in Fig. 4f, PT32bT of $N_{FR} = 2$ and other polymers of even $N_{FR}$ manage to decrease such unfavorable electron hopping through a reduction in the wavefunction components on the $\alpha$-C sites away from bridge bonds. However, $E_{LUMO}$ inevitably increases after a couple of odd and even alternations of $N_{FR}$. In the $N_{FR} = \infty$ limit, $E_{LUMO}$ and consequently $E_g$ experience a sudden energy jump due to the lack of favorable electron hopping across bridge bonds in PTA.

Opposite to the LUMO case, the HOMO wavefunction of PTh (Fig. 3, V band) has nodes on the S sites. Therefore, increasing $N_{FR}$ by adding more sulfur sites does not change $E_{HOMO}$ as much as $E_{LUMO}$. However, as $N_{FR}$ increases, the $\alpha$-C wavefunction components in the L band (Fig. 3) also increase such that the L band starts to delocalize and its energy becomes dispersed. As the energy dispersion of the L band increases, it eventually overtakes
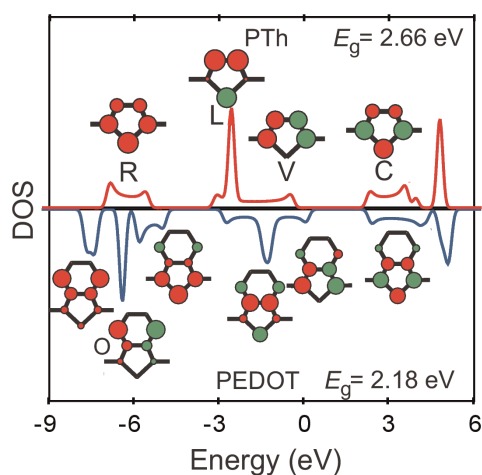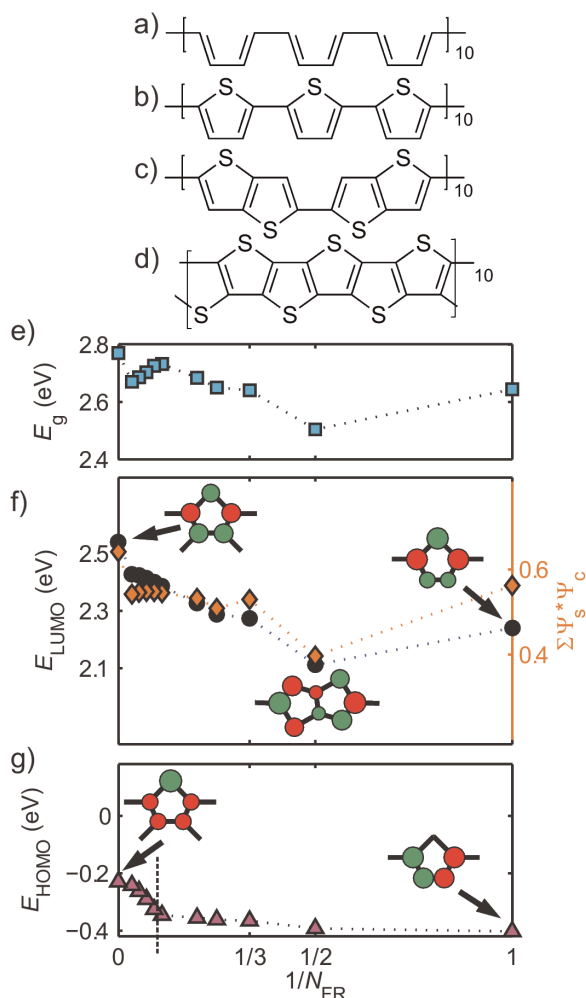
**Figure 4. PTh (b), PT32bT (c), and PTA (d) share the identical conjugated carbon backbone (a) with an equal amount of carbon atoms along the conjugated path, for instance $N = 120$ as shown.** The computed optical band gap (e) and energies of LUMO (f) and HOMO (g) as a function of the number of fused rings in their oligomers, where $N_{FR} = 1$ for PTh, 2 for PT32bT, and $\infty$ for PTA. Unfavorable electron hopping between S and $\alpha$-C are plotted as orange diamonds in (f) on the right y-axis.
doi:10.1371/journal.pone.0086370.g004

the V band and becomes the new HOMO state. Such an L-V band energy crossover occurs around $N_{FR} = 7$ for our $N = 120$ case, after which $E_{HOMO}$ increases sharply (Fig. 4g).

In summary, since the largest $E_g$ drop is 0.14 eV from PTh to PT32bT (Fig. 4e), the intention to lower the optical bandgap of PTh by using fused rings parallel to the conjugated path would not reach the 1.20 eV bandgap target. As a pleasant surprise, however, the enhanced wavefunction components on the bridge C sites, similar to the PT32bT case shown in Fig. 4f, help greatly in reducing the bandgaps of copolymers as will be discussed in the copolymer section.

## Perpendicular Fused Rings

The predicted optical gaps for this group are shown in Fig. 2c with $R^2 = 0.77$, $ME = -0.08$ eV, and $MAD = 0.21$ eV. The worst result is for poly-2,3-dihexylthieno[3,4-b]pyrazine (DHTP) [53], with a calculated optical gap nearly 35% higher than from experiments. The poor result of DHTP comes from a combination

of two factors: 1) the experiments were done with long polymers that have a tendency to aggregate and thus introduce inter-chain effects and 2) despite attempts to chemically dedope the polymer, it remained paramagnetic, indicating a residual doping that decreases the measured gap.

The important contribution of the perpendicular fused rings series to the aSSH model is in determining a new bridge bond $\gamma$ that is dependent on the structure of the monomers being connected. To understand the need for this, we can take poly-isothianaphthene (PITN) as an example. The lower optical bandgap of PITN as compared to PTh is typically attributed to the quinoid (reversed bond orders as compared to aromatic) character of the PITN backbone. [54] This extends from a comparison to tPA systems in which an "aromatic" and a "quinoid" dimerization (which in tPA are degenerate) are connected in reaction space by a non-dimerized form with a vanishing gap. Following this idea, simply reducing the aromatic or quinoid character towards a non-dimerized backbone would lead to a reduction in the gap. It follows that if the dimerization of the backbone is responsible for lowering the gap, we should expect the gap to lower at a faster rate with increasing chain (backbone) length. This trend is not what we observe between PTh and PITN.

In systems such as PITN with aromatic rings fused perpendicular to the conjugated pathway, the monomers themselves have lower bandgaps simply due to energy level splitting. Fig. 5 shows the energy level splitting for poly-isothianaphthene (PITN), [55] depicted as a combination of Th and benzene (Bz) orbitals sharing two carbons. Although the ITN monomer has a bandgap nearly 2 eV smaller than the Th monomer, the bandgap of PITN (Fig. 5, blue squares) is only 0.8 eV smaller than PTh (Fig. 5, yellow circles), indicating that the highly aromatic ITN unit actually has a smaller electronic overlap with neighboring units. In other words, the lower gap of the polymer is due to the lower starting point of the monomer overcoming a weaker polymerization effect. This effect is exacerbated in poly-(9,10-anthrylene vinylene) (PATV), which uses anthracene as its monomer with three fused rings perpendicular to the chain direction. Although the ATV monomer has a bandgap even lower than ITN, polymerization does not significantly lower the bandgap any further (Fig. 5, purple diamonds). Using the optical gap slope with respect to the chain length of PITN and PATV, we obtain the $\gamma$ parameters of 0.75 and 0.2 for perpendicular fused rings of size two and three, respectively.

In order to decrease the bandgaps for polymers consisting of perpendicular fused rings we must to enhance the electron hopping between the connected monomers. This enhancement can be achieved by introducing parallel fused ring monomers between each perpendicular fused ring monomer to form copolymers, examples of which are discussed in the copolymers section.

## Copolymers

Copolymers of donor-acceptor units have been leading the way in improving organic PV efficiency from 5% to 9%. [56] Despite using the same parameters as used on the much simpler structures, the copolymers group show agreement (depicted in Fig. 2d) with experimental values of $R^2 = 0.82$, $MAD = 0.15$ eV, and $ME = 0.04$ eV, on par with the other groups in this study. The calculations demonstrate that, as shown in Fig. 6, copolymers (triangles) with small conjugation lengths $N_C$ do not necessarily have lower bandgaps than their parent regioregular polymers (circles or squares) of the same $N_C$, where $N_C$ is the number of carbon atoms along the conjugated pathway. The lower bandgaps in longer chain lengths are due to stronger polymerization effects,
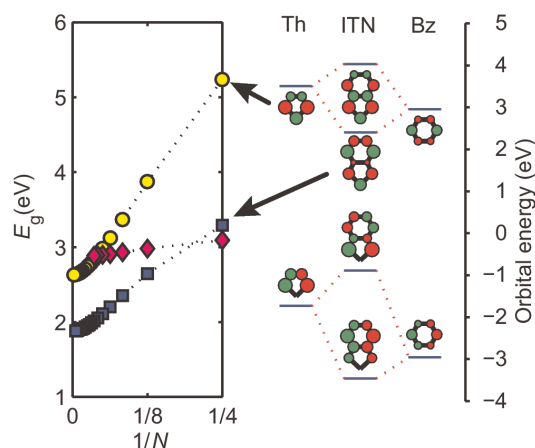
**Figure 5. Bandgap as a function of the $\pi$-conjugated length $N$ for PTh (yellow circles), PITN (blue squares), and PATV (purple diamonds).** The bandgap of ITN is 2 eV lower than Th because of the energy level splitting between Th and Bz.
doi:10.1371/journal.pone.0086370.g005

through the parallel fused rings that strengthen electronic communications between perpendicularly fused units. This effect is valid even when combining two typical acceptors (electron poor units), such as benzo[1,2-b:4,3-b']dithiophene (BDT) (Fig. 6a, gray diamonds) and benzobisthiadiazole (BBTD) (Fig. 6c, red circles), for which case a bandgap of 1.4 eV is predicted (magenta triangles). Furthermore, our calculations clearly show that there are no real electronic distinctions between donor and acceptor units in co-polymers, since upon photoexcitations the localized excitonic electron- and hole-wavefunctions span over both the Tt donor (Fig. 6b, green squares) and BDT acceptor units along the same $\pi$-conjugated polymer backbone as shown in Fig. 6e. Our calculations also indicate that these copolymers do not form two separated domain walls of irrational charges. [57] As a sharp contrast, the electron and hole states can be spontaneously separated across the fullerene-polymer heterojunctions through $\pi$-$\pi$ stacking (Fig. 6f). [25] With this in mind, we further propose to replace the N atoms in BBTD with carbons (Fig. 6d, blue squares) to form a copolymer that reaches the 1.2 eV target (cyan triangles). When taking into account that favorable $\pi$-$\pi$ stacking effects can lower the bandgap by a further 0.4 eV, [25] our calculations suggest that an optical bandgap as low as 0.8 eV may be possible, making it a candidate for the long wavelength absorbing materials in tandem OPV cells.

## Polycyclic Aromatic Hydrocarbons

PAHs are essentially flakes of graphene, the Fermi energy of which varies linearly with wavevector through the Dirac point without undergoing the Peierls dimerization [58,59]. In short polyacenes, nonacene ($N_R = 9$) being the longest ever synthesized to date [60,61], the inevitable edge dimerization effects lead to the characteristic bond-centered HOMO and LUMO phase patterns near the edges (Fig. 7a) that open their bandgaps. For pentacene ($N_R = 5$), we find $E_g = 1.8$ eV. For much longer polyacenes, the ground state may be an open shell singlet diradical [62], so our discussions will be limited to the shorter molecules. The agreement with experimental values is shown in Fig. 2e, with $R^2 = 0.97$, $MAD = 0.28$ eV, $ME = -0.27$ eV. The relatively high $MAD$ value is due to the high $ME$ value, a consequence of choosing $\gamma = 1.16$ for all benzene-type rings to simplify usage of the model.
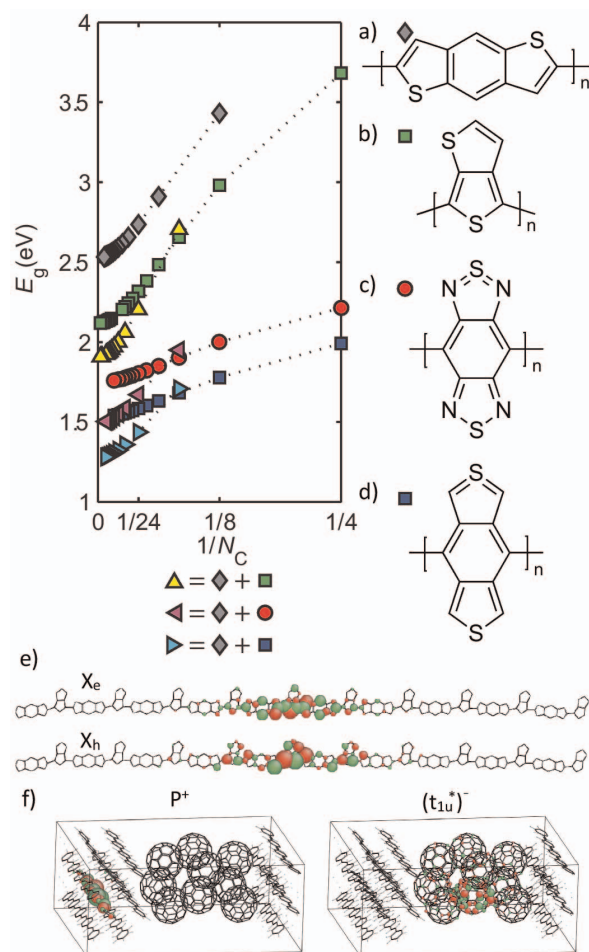


**Figure 6. Bandgaps of copolymers and their parent regioregular polymers, including BDT of parallel fused rings (gray diamonds), Tt (green squares), BBTD (red circles), and BBT (blue squares).** $N_C$ is the number of carbon atoms in the conjugated pathway. The yellow up-triangles, magenta left-triangles, and cyan right-triangles are copolymers of BDT with Tt, BBTD, and BBT, respectively. Copolymers show steep bandgap reductions via polymerization. (e) Excitons in copolymers do not show spontaneous charge separations, where the electron $X_e$ and hole $X_h$ states extend over both the BDT and Tt units. (f) In contrast, spontaneous charge separations occur at the bulk heterojunction interfaces, leaving behind a hole polaron state $P^+$ in the polymer phase and an electron state $(t_{1u}^*)^-$ in the $C_{60}$ phase.
doi:10.1371/journal.pone.0086370.g006

The trends are nevertheless correct, demonstrated by the $R^2$ near unity.

In order to reduce the optical gap of polyacenes, one can create nodes on the $\beta$ sites (the carbons shared by the rings) by fusing 5 membered rings to the ends. Common in all 5-membered aromatic rings [23], the HOMO level of Th (Fig. 3, V band) is bonding between $\alpha$-$\beta$ sites and anti-bonding between $\beta$-$\beta$ sites and has nodes on S sites. When fusing Th to anthracene of $N_R = 3$ (Fig. 7b), the two $\alpha$-C's of Th naturally extend the non-bonding wavefunction phase pattern of polyacenes to new S edges and leave nodes precisely on $\beta$ sites. This effectively shifts the HOMO level up to the Dirac point and reduces $E_g$ from 1.8 to 1.1 eV. Alternatively, one may substitute the $\alpha$-C's of Th with N's to form a similar structure to the thiadiazole units in BBTD (Fig. 6c). This gives an $E_g$ of 1.21 eV.
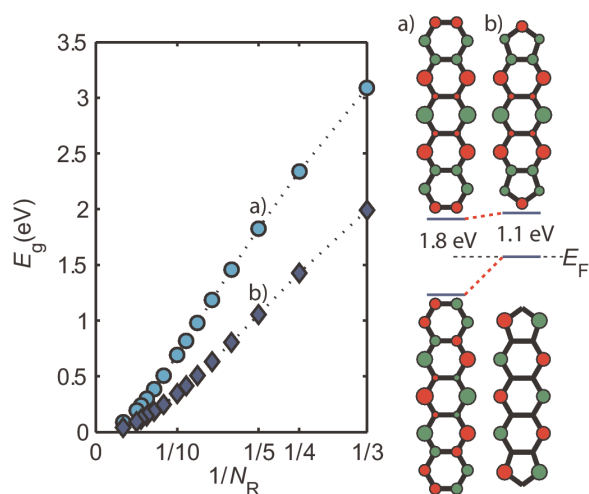
**Figure 7. Bandgap comparison between polyacenes and thiophene capped polyacenes as a function of the number of aromatic rings** $N_R$. The latter have lower bandgaps for comparable molecular sizes. As an example, the HOMO and LUMO levels of pentacene (a) is compared with thiophene capped anthracene (b), showing how the reduction in the wavefunction of the shared carbon sites on the HOMO is mostly responsible for the bandgap differences.
doi:10.1371/journal.pone.0086370.g007

## Conclusion

The accurate prediction of the optical bandgap of a generic materials system will remain as a grand challenge in condensed matter theory. Working towards that goal, we demonstrate a model Hamiltonian for virtually all the major types of $\pi$-conjugated systems in which electron correlations are renormalized into quasi-particles through the universal, and therefore transferable, electron-phonon coupling parameters [11,19,23,24]. With excellent agreement to their corresponding experimental measurements over a comprehensive data set, our results indicate that residual correlation effects beyond such universal electron-phonon couplings are not essential as far as the optical bandgaps are concerned. Similarly, and corroborated by the fused thiophene series, we find the lack of explicit planarity to have a negligible impact on the accuracy of the model. The aSSH Hamiltonian is an accurate, transferable, and efficient computational tool that provides the quantitative description of structure-property relationships afforded by quantum mechanical theories.

From our calculations, the strategies of planarization or simple substitutions did not lead to the target optical gaps 1.2 eV. To reach the desired gaps, we suggest a copolymer of parallel and perpendicular monomers (both benzodithiophenes), which we find in general to be the best strategy by taking advantage of both the lower monomer gaps of perpendicular units and the enhanced electronic communication of the parallel ones. We also propose a small molecule oligomer (a thiophene capped anthracene) that arises from our analysis of PAHs, in particular of pentacene, with the aSSH model giving insights into the electronic structure of the molecules and how to modify them for lower gaps. With these examples, we put forth the aSSH model as an in-silico design tool to guide the search for optimized organic electronics.

## Supporting Information

**Figure S1  Skeletal formulae of simple ring systems.**
Simple ring systems consist of monomers that are single aromatic rings that may contain single atoms or non-conjugated rings attached.
(PDF)

**Figure S2  Skeletal formulae of parallel fused ring systems.** Parallel fused ring systems consist of monomers wherein two or more aromatic rings are fused and all rings are part of the main conjugated pathway.
(PDF)

**Figure S3  Skeletal formulae of perpendicular fused ring systems.** Perpendicular fused ring systems consist of monomers wherein two or more aromatic rings are fused, but only one of the rings is connected to the main conjugated pathway.
(PDF)

**Figure S4  Skeletal formulae of polycyclic aromatic hydrocarbons and derivatives.** Polycyclic aromatic hydrocarbons are made entirely of fused aromatic carbon rings, while derivatives include simple heteroatom substitutions for hydrogen.
(PDF)

**Figure S5  Skeletal formulae of copolymers.** Copolymers refer to any system made of more than one type of monomer.
(PDF)

**Figure S6  Skeletal formulae of $\pi$-$\pi$ stacking systems.** The $\pi$-$\pi$ stacking systems consist of multiple separate oligomers necessitating an inter-chain interaction term.
(PDF)

**Table S1  Experimental and aSSH calculated optical gaps for simple ring polymers.**
(PDF)

**Table S2  Experimental and aSSH calculated optical gaps for parallel fused ring systems.**
(PDF)

**Table S3  Experimental and aSSH calculated optical gaps for perpendicular fused ring systems.**
(PDF)

**Table S4  Experimental and aSSH calculated optical gaps for polycyclic aromatic hydrocarbons and derivatives.**
(PDF)

**Table S5  Experimental and aSSH calculated optical gaps for copolymers.**
(PDF)

**Table S6  Experimental and aSSH calculated optical gaps for $\pi$-$\pi$ stacking systems.**
(PDF)

**References S1  References for data contained in Tables S1–6.** Although some references for the Supporting Information may be the same as for the main article, their reference numbers may not be the same.
(PDF)

## Author Contributions

Conceived and designed the experiments: ALB YS JL XL. Performed the experiments: ALB YS JL. Analyzed the data: ALB YS JL XL. Contributed reagents/materials/analysis tools: ALB YS XL. Wrote the paper: ALB.

# References

1. Burroughes JH, Jones CA, Friend RH (1988) New semiconductor device physics in polymer diodes and transistors. Nature 335: 137–141.

2. Yu G, Gao J, Hummelen JC, Wudl F, Heeger AJ (1995) Polymer photovoltaic cells: Enhanced efficiencies via a network of internal donor-acceptor heterojunctions. Science 270: 1789–1791.

3. Scharber M, Mhlbacher D, Koppe M, Denk P, Waldauf C, et al. (2006) Design rules for donors in BulkHeterojunction solar CellsTowards 10% EnergyConversion efficiency. Advanced Materials 18: 789–794.

4. Roncali J (2007) Molecular engineering of the band gap of pi-conjugated systems: Facing technological applications. Macromolecular Rapid Communications 28: 1761–1775.

5. Blouin N, Michaud A, Gendron D, Wakim S, Blair E, et al. (2008) Toward a rational design of poly(2,7-carbazole) derivatives for solar cells. Journal of American Chemical Society 130: 732–742.

6. Mattuck RD (1976) A Guide to Feynman Diagrams in the Many-Body Problem. New York: McGraw-Hill, 2 edition.

7. Hohenberg P, Kohn W (1964) Inhomogeneous electron gas. Physical Review 136: B864–B871.

8. Kohn W (1999) Nobel leture: Electronic structure of matter – wave functions and density functionals. Reviews of Modern Physics 71: 1253–1266.

9. Parr RG, Yang W (1989) Density-Functional Theory of Atoms and Molecules. The International Series of Monographs on Chemistry. New York: Oxford University.

10. Cohen AJ, Mori-Sanchez P, Yang W (2008) Insights into current limitations of density functional theory. Science 321: 792–794.

11. Heeger AJ, Kivelson S, Schrieffer JR, Su WP (1988) Solitons in conducting polymers. Reviews of Modern Physics 60: 781–851.

12. Runge E, Gross EKU (1984) Density-functional theory for time-dependent systems. Physical Review Letters 52: 997–1000.

13. van Faassen M, de Boeij PL, van Leeuwen R, Berger JA, Snijders JG (2002) Ultranonlocality in time-dependent current-density-functional theory: Application to conjugated polymers. Physical Review Letters 88: 186401.

14. Lee Y, Kertesz M (1988) The effect of heteroatomic substitutions on the band gap of polyacetylene and polyparaphenylene derivatives. The Journal of Chemical Physics 88: 2609–2617.

15. Hong SY, Marynick DS (1992) Modified extended hckel band calculations on conjugated polymers. The Journal of Chemical Physics 96: 5497–5504.

16. Eckhardt H, Shacklette LW, Jen KY, Elsenbaumer RL (1989) The electronic and electrochemical properties of poly(phenylene vinylenes) and poly(thienylene vinylenes): An experimental and theoretical study. The Journal of Chemical Physics 91: 1303–1315.

17. Quattrocchi C, Lazzaroni R, Bredas JL, Zamboni R, Taliani C (1993) Theoretical investigation of the structure and electronic properties of poly(dithieno[3,4-b:3′,4′-d]thiophene), a small-band-gap conjugated polymer. Macromolecules 26: 1260–1264.

18. Yang S, Olishevski P, Kertesz M (2004) Bandgap calculations for conjugated polymers. Synthetic Metals 141: 171–177.

19. Su WP, Schrieffer JR, Heeger AJ (1979) Solitons in polyacetylene. Physical Review Letters 42: 1698–1701.

20. Longuet-Higgins HC, Salem L (1959) The alternation of bond lengths in long conjugated chain molecules. Proceedings of the Royal Society of London Series A Mathematical and Physical Sciences 251: 172–185.

21. Kuzmany H, Mehring M, Roth S, editors (1989) Electronic properties of conjugated polymers III : basic models and applications : international winterschool, Kirchberg, Tirol, March 11–18, 1989. Number 91 in Springer series in solid-state sciences. Berlin; New York: Springer-Verlag.

22. Krti J, Kuzmany H (1991) Resonance raman scattering from finite and infinite polymer chains. Physical Review B 44: 597–613.

23. Li M, Lin X (2010) Adapted Su-Schrieffer-Heeger hamiltonian for polypyrrole. Physical Review B 82: 155141.

24. Botelho AL, Shin Y, Li M, Jiang L, Lin X (2011) Unified hamiltonian for conducting polymers. Journal of Physics: Condensed Matter 23: 455501.

25. Shin Y, Lin X (2013) Modeling photoinduced charge transfer across π-conjugated heterojunctions. The Journal of Physical Chemistry C 117: 12432–12437.

26. Subbaswamy KR, Grabowski M (1981) Bond alternation, on-site coulomb correlations, and solitons in polyacetylene. Physical Review B 24: 2168–2173.

27. Lin X, Föerst C, Li J, Yip S (2006) Multiple self-localized electronic states in trans-polyacetylene. Proceedings of the National Academy of Sciences of the United States of America 103: 8943–8946.

28. Lin X, Li J, Yip S (2005) Controlling bending and twisting of conjugated polymers via solitons. Physical Review Letters 95: 198303.

29. Shockley W, Queisser HJ (1961) Detailed balance limit of efficiency of p-n junction solar cells. Journal of Applied Physics 32: 510–519.

30. Gunes S, Neugebauer H, Sariciftci NS (2007) Conjugated polymer-based organic solar cells. Chemical Review 107: 1324–1338.

31. Li G, Zhu R, Yang Y (2012) Polymer solar cells. Nature Photonics 6: 153–161.

32. Yang F, Shtein M, Forrest SR (2005) Controlled growth of a molecular bulk heterojunction photovoltaic cell. Nature Materials 4: 37–41.

33. Price SC, Stuart AC, You W (2010) Low band gap polymers based on benzo[1,2-b:4,5-b′]]dithiophene: Rational design of polymers leads to high photovoltaic performance. Macromolecules 43: 4609–4612.

34. Price SC, Stuart AC, You W (2011) Development of fluorinated benzothiadiazole as a structural unit for a polymer solar cell of 7%efficiency. Angew Chem Int Ed 50: 2995–2998.

35. Hellström S, Zhang FL, Inganäs O, Andersson MR (2009) Structure-property relationships of small bandgap conjugated polymers for solar cells. Dalton Trans 2009: 10032–10039.

36. Gidron O, Diskin-Posner Y, Bendikov M (2010) α-Oligofurans. Journal of the American Chemical Society 132: 2148–2150.

37. Walker IC, Palmer MH, Hopkirk A (1989) The electronic states of the azines. II. Pyridine, studied by VUV absorption, near-threshold electron energy loss spectroscopy and ab initio multi-reference configuration interaction calculations. Chemical Physics 141: 365–378.

38. Guo X, Ortiz RP, Zheng Y, Kim MG, Zhang S, et al. (2011) Thieno[3,4-c]pyrrole-4,6-dione-based polymer semiconductors: Toward high-performance, air-stable organic thin-film transistors. Journal of American Chemical Society 133: 13685–13697.

39. Shimizu Y, Shen Z, Ito S, Uno H, Daub J, et al. (2002) A convenient synthesis of isothianaphthene oligomers and their electrochemical studies. Tetrahedron Letters 43: 8485–8488.

40. Quattrocchi C, Lazzaroni R, Bredas JL, Kiebooms R, Vanderzande D, et al. (1995) Optical absorption spectra of aromatic isothianaphthene oligomers: Theory and experiment. Journal of Physical Chemistry 99: 3932–3938.

41. Pople JA, HeadGordon M, Raghavachari K (1987) Quadratic configuration interaction. a general technique for determining electron correlation energies. The Journal of Chemical Physics 87: 5968.

42. Davis W, Svec W, Ratner M, Wasielewsk M (1998) Molecular-wire behaviour in p-phenylenevinylene oligomers. Nature 396: 60.

43. Diaz A, Crowley J, Bargon J, Gardini G, Torrance J (1981) Electrooxidation of aromatic oligomers and conducting polymers. Journal of Electroanalytical Chemistry 121: 355–361.

44. Andrews L, Kelsall B, Blankenship T (1982) Vibronic absorption spectra of naphthalene and substituted naphthalene cations in solid argon. The Journal of Physical Chemistry 86: 2916–2926.

45. Chandross EA, Ferguson J, McRae EG (1966) Absorption and emission spectra of anthracene dimers. The Journal of Chemical Physics 45: 3546.

46. Hinderhofer A, Heinemeyer U, Gerlach A, Kowarik S, Jacobs R, et al. (2007) Optical properties of pentacene and perfluoropentacene thin films. The Journal of Chemical Physics 127: 194705.

47. Payne M, Parkin S, Anthony J (2005) Functionalized higher acenes: Hexacene and heptacene. Journal of the American Chemical Society 127: 8028–8029.

48. Rang Z, Haraldsson A, Kim D, Ruden P, Nathan M, et al. (2001) Hydrostatic-pressure dependence of the photoconductivity of single-crystal pentacene and tetracene. Applied Physics Letters 79: 2731.

49. Becker RS, Singh IS, Jackson EA (1963) Comprehensive spectroscopic investigation of polynuclear aromatic hydrocarbons. I. Absorption spectra and state assignments for the tetracyclic hydrocarbons and their alkylsubstituted derivatives. The Journal of Chemical Physics 38: 2144–2171.

50. Khan ZH, Khanna BN (1973) Electronic absorption spectra of pyrene and its monopositive ion. The Journal of Chemical Physics 59: 3015–3019.

51. Sariciftci NS, Smilowitz L, Heeger AJ, Wudl F (1992) Photoinduced electron transfer from a conducting polymer to buckminsterfullerene. Science 258: 1474–1476.

52. Lin X, Li J, Smela E, Yip S (2005) Polaron-induced conformation change of a single polypyrrole chain: An intrinsic actuation mechanism. International Journal of Quantum Chemistry 102: 980–985.

53. Pomerantz M, Chaloner-Gill B, Harding LO, Tseng JJ, Pomerantz WJ (1993) New processable low band-gap, conjugated polyheterocycles. Synthetic Metals 55: 960–965.

54. Kertesz M, Choi CH, Yang S (2005) Conjugated polymers and aromaticity. Chem Rev 105: 3448–3481.

55. Wudl F, Kobayashi M, Heeger AJ (1984) Poly(isothianaphthene). The Journal of Organic Chemistry 49: 3382–3384.

56. Risko C, McGehee MD, Brdas J (2011) A quantum-chemical perspective into low optical-gap polymers for highly-efficient organic solar cells. Chem Sci 2: 1200–1218.

57. Rice MJ, Mele EJ (1982) Elementary excitations of a linearly conjugated diatomic polymer. Physical Review Letters 49: 1455–1459.

58. Peierls RE (1955) Quantum Theory of Solids. The International series of monographs on physics. New York: Oxford University Press.

59. Li M, Lin X (2010) Twin distortions of the peierls instability. Physical Review B 81: 153102.

60. Kaur I, Jazdzyk M, Stein NN, Prusevich P, Miller GP (2010) Design, synthesis, and characterization of a persistent nonacene derivative. Journal of the American Chemical Society 132: 1261–1263.

61. Tnshoff C, Bettinger H (2010) Photogeneration of octacene and nonacene. Angewandte Chemie International Edition 49: 4125–4128.

62. Bendikov M, Duong HM, Starkey K, Houk KN, Carter EA, et al. (2004) Oligoacenes: Theoretical prediction of open-shell singlet diradical ground states. Journal of the American Chemical Society 126: 7416–7417.